NANO LETTERS

Letter

pubs.acs.org/NanoLett

Atomic-Scale Imaging of Cation Ordering in Inverse Spinel Zn_2SnO_4 Nanowires

Lihong Bao,[†,§] Jianfeng Zang,[†,∥] Guofeng Wang,[‡] and Xiaodong Li*[,†]

[†]Department of Mechanical Engineering, University of South Carolina, Columbia, South Carolina 29208, United States

[‡]Department of Mechanical Engineering and Materials Science, University of Pittsburgh, Pittsburgh, Pennsylvania 46202, United States

Supporting Information

ABSTRACT: By using high-angle annular dark-field scanning transmission electron microscopy (HAADF-STEM) coupled with density functional theory (DFT) calculations, we demonstrate the atomic-level imaging of cation ordering in inverse spinel Zn_2SnO_4 nanowires. This cation ordering was identified as 1:1 ordering of Zn^{2+} and Sn^{4+} at the octahedral sites of the inverse spinel crystal with microscopic symmetry transition from original cubic $Fd\bar{3}m$ to orthorhombic *Imma* group. This ordering generated a 67.8% increase in the elastic modulus and 1−2 order of magnitude lower in the electric conductivity and electron mobility compared to their bulk counterpart.

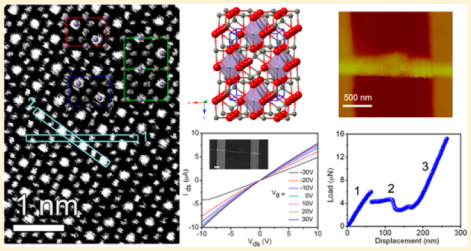

KEYWORDS: *Cation ordering, inverse spinel, scanning transmission electron microscopy (STEM), density functional theory (DFT) calculations*

Cation ordering/disordering plays a critical role in tuning the crystal structure, stability, and properties of spinel oxides.[1−7] The ordered/disordered cation arrangements originate from partial inversion of normal spinels[8] by cation self-diffusion[9] or substitution,[10−12] or from configuration of the degrees of freedom of cations in octahedral sites of inverse spinels.[2,13−16] Hass systematically studied this cation ordering in spinel structures[17] using symmetrical rules based on Landau's theory of phase transitions.[18] However, the specific short-range order is difficult to be determined by standard diffraction techniques, such as X-ray[19,20] and neutron diffractions,[21] because they can only yield overall site occupation ratios based on the refinement of obtained spectra, while local distribution of cations could vary appreciably. Polarized Raman spectroscopy is capable of detecting symmetry-broken enabled extra vibrational modes induced by cation ordering, but it determines cation ordering in an indirect way with the help of symmetrical analysis.[14] Direct atomic-level visualization of ordered/disordered arrangements of cations is of both scientific and technological importance for an in-depth understanding of atomic scale phase transition in spinels and tailoring their properties for device applications.

Development in aberration-corrected scanning transmission electron microscopy (STEM)[22,23] enables subangstrom resolved imaging of cation arrangements in spinels and other complex oxides[7,8,24] due to its extreme sensitivity to the atomic numbers (Z-contrast). Zn_2SnO_4 (ZTO), as an important member of transparent conducting oxides (TCOs),[25] has attracted great attention due to its excellent electronic, optical, and optoelectronic properties, and potential applications in transparent electrodes, photovoltaic devices, lithium batteries, and sensors.[26−28] Previous theoretical calculations predicted that ZTO possesses an inverse spinel structure (space group: $Fd\bar{3}m$, No. 227, $Z = 8$) with all tetrahedral A sites (8a) occupied by Zn^{2+} cations, while the octahedral B sites (16d) occupied randomly by both Zn^{2+} and Sn^{4+} cations in equal proportions,[3,16,29] as schematically shown in Figure 1. However, whether Zn^{2+} and Sn^{4+} are distributed in a random manner among B sites or present specific short-range ordering have not been determined experimentally although theoretical calculations predicted a $P4_122$ tetragonal cation ordering in ground state.[16,29]

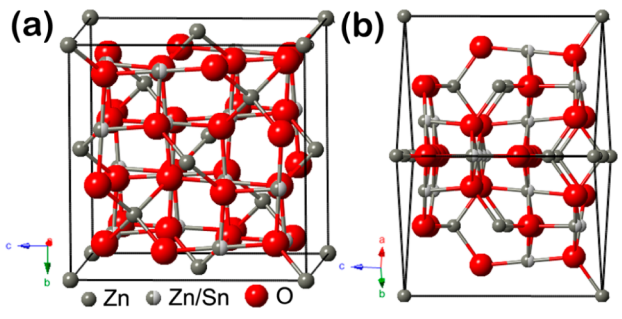

Figure 1. (a) Ball−stick model of inverse spinel Zn_2SnO_4 (ZTO), showing randomly distributed Zn^{2+} and Sn^{4+} cations at octahedral B sites. (b) ZTO atomic structure projected along the [110] direction, showing that all tetrahedral A sites are occupied by Zn cations and octahedral B sites are occupied by Zn and Sn cations randomly in equal proportions.

Received: August 10, 2014
Revised: September 21, 2014
Published: October 9, 2014

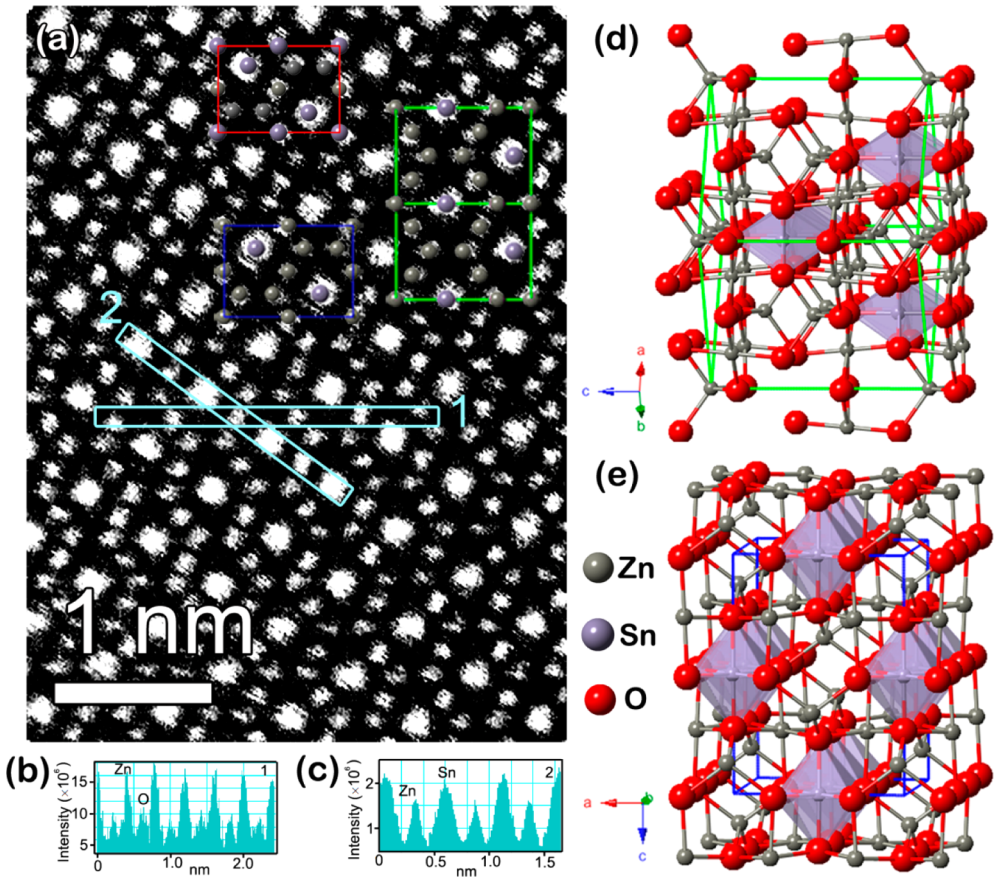

Figure 2. (a) HAADF-STEM image of ZTO projected along the [110] direction shows a *Z*-sensitive contrast of Sn and Zn columns, indicating ordered distribution of Zn^{2+} and Sn^{4+} at octahedral B sites. Two-dimensional Zn and Sn atomic arrays (green frame) fitted with the ordered cation arrangement are superimposed on the STEM image. Two other Zn and Sn atomic arrays with microscopic symmetries of tetrahedral $P4_122$ (red frame) and orthorhombic *Imma* (blue frame) regarding cation ordering in inverse ZTO are also superimposed on the STEM image, showing orthorhombic *Imma* ordering is consistent with the STEM image. (b,c) Line intensity profiles for the atom columns at octahedral B sites indicated in panel a as rectangular frames 1 and 2, respectively. (d) Unit cell representing ordered Zn and Sn arrangements at octahedral B sites in STEM image in panel a. (e) Cation ordered unit cell with orthorhombic *Imma* symmetry in accordance with STEM image in panel a.

In this letter, we demonstrate the direct atomic-level visualization of cation ordering in inverse spinel ZTO nanowires. In particular, using HAADF-STEM technique coupled with DFT calculations, we identified this ordering as 1:1 ordering of Zn^{2+} and Sn^{4+} at the octahedral sites of inverse spinel ZTO with microscopic symmetry transition from original cubic $Fd\bar{3}m$ to orthorhombic *Imma* group. Moreover, this ordering induced a 67.8% increase in the elastic modulus and 1−2 orders of magnitude lower in the electric conductivity and electron mobility compared to their bulk counterpart.

ZTO nanowires were prepared by a simple chemical vapor deposition method, which is described in detail elsewhere.[30] The atomic-resolution imaging of cation ordering was performed on a JEOL-2010F HRTEM with a Fischione HAADF detector and a spherical abberation corrector (CEOS GmbH, Germany) operated at 200 keV. All the electronic structure calculations were carried out by using Vienna Ab-initio Simulation Package (VASP) code and with the projector augmented wave (PAW) approach. In these calculations, we used the generalized gradient approximation (GGA) with PW91 functional by Perdew and co-workers for evaluating exchange-correlation energy; set the plane-wave cutoff energy as 500 eV; and employed a 3 × 3 × 3 Monkhorst−Pack *k*-point mesh for Brillouin zone integration. Mechanical properties were measured by an atomic force microscopy (AFM)-based three-point bending method with the contact/indentation mode, and electrical properties were extracted from ZTO nanowire based field-effect transistors (FETs).

Figure 2a shows a HAADF-STEM image in the [110] projection of a ZTO nanowire. As Sn has a larger atomic number (Z = 50) than Zn (Z = 29), the Sn−Sn (Sn−Zn) columns are much brighter than Zn−Zn columns. This sensitive *Z*-dependent contrast between different atomic columns is verified by relative intensity differences of B site columns, which is denoted by the light blue rectangles in Figure 2a, and detailed line intensity profiles shown in Figure 2b. O is too light to be imaged (Z = 8) compared with Sn and Zn although the line profile of "1" in Figure 2b shows resolved intensities for O. The clearly resolved Zn and Sn atomic arrays in Figure 2a indicates that all tetrahedral A sites are occupied by Zn, while the octahedral B sites are occupied by Zn and Sn in an ordered manner, which is consistent with the site occupations shown in Figure 1b except for the cation arrangement differences at B sites due to specific ordering. Geometry analysis suggests that there are in total 21 possible configurations of Zn and Sn at octahedral B sites with this specific ordered arrangement on the top projection of [110]. In this study, we used the DFT method to calculate the energies of these 21 configurations of bulk ZTO crystal. Our DFT results

dx.doi.org/10.1021/nl503077y | *Nano Lett.* 2014, 14, 6505−6509

revealed that this ordered configuration (as shown in Figure 2d) had the lowest potential energy among the 21 configurations examined. It was predicted that the ZTO crystal with an inverse spinel structure and this specified cation ordering would have an equilibrium lattice parameter of 8.80 Å and energy of about 0.77 eV (per ZTO formula) lower than the relaxed ZTO crystal with a normal spinel structure and lattice parameter of 8.76 Å. The Zn and Sn atomic arrays with this ordering (green frame) is superimposed on the STEM image (Figure 2a), and the corresponding unit cell is shown in Figure 2d. On the basis of symmetrical considerations, this ordered configuration can be represented by an *Imma* orthorhombic structure. Zn and Sn atomic arrays with the *Imma* ordering (blue frame) are superimposed on the STEM image in Figure 2a, revealing that *Imma* ordering arrangement is consistent with the STEM image. Hass predicted that only two types of 1:1 ordering of A and B cations, tetrahedral $P4_122$ type and orthorhombic *Imma* type, are allowed in inverse spinels.[17] Zn and Sn atomic arrays with $P4_122$ ordering (red frame) are also superimposed on the STEM image in Figure 2a, indicating apparent disagreement with the STEM image. Both tetrahedral $P4_122$ and orthorhombic *Imma* unit cells are two times smaller than its original cubic unit cell ($Fd\bar{3}m$) with lattice parameters of $\vec{a} = 1/2(\vec{a}_c + \vec{b}_c)$, $\vec{b} = 1/2(\vec{a}_c - \vec{b}_c)$, and $\vec{c} = \vec{c}_c$. The equivalent atomic sites of cubic $Fd\bar{3}m$, tetrahedral $P4_122$, and orthorhombic *Imma* are listed in Table 1. The orthorhombic *Imma*

Table 1. Atomic Site Symmetries of $Fd\bar{3}m$, Ordered $P4_122$, and *Imma* Structures of Zn_2SnO_4

$Fd\bar{3}m$ (cubic)		$P4_122$ (tetragonal)		*Imma* (orthorhombic)	
atom	Wyckoff index	atom	Wyckoff index	atom	Wyckoff index
Zn (1)	8a	Zn (1)	4c	Zn (1)	4e
Zn (2)/Sn	16d	Sn	4a	Sn	4b
O	32e	Zn (2)	4b	Zn (2)	4c
		O (1)	8d	O (1)	8h
		O (2)	8d	O (2)	8i

unit cell (Figure 2e) shows that one characteristic of this cation ordering is the formation of ···—Sn—Sn—Sn—··· chains along [110] direction (Sn polyhedrons in Figure 2e). This Sn atom chain formation has important implications on electrical transport properties of ZTO because these chains provide highways for electron transport, and extended conduction bands are formed from strong cation—cation interactions through overlapping of vacant s orbitals between neighboring cations.[4]

Full relaxation of the orthorhombic *Imma* unit cell indicated that this ordering will inevitably induce distortion of O sublattices, which results in Zn^{tetra}—O, Zn^{octa}—O, and Sn^{octa}—O bond length elongation/contraction and generates internal strain in ZTO crystal to mechanically stiffen ZTO nanowires. Table 2 indicates the effects of this *Imma* orthorhombic ordering on cation bond lengths between tetrahedral and octahedral cation sites and their oxygen nearest neighbors. The bond length between tetrahedral Zn sites and their oxygen nearest neighbors is contracted from 2.098 to 2.010 Å, while those of octahedral Zn and Sn sites are elongated from 2.041 to 2.120 and 2.068 Å, respectively. For comparison, the bond lengths of tetrahedral $P4_122$ ordering are also listed in Table 2. To experimentally investigate this cation ordering on the

Table 2. Tetrahedral and Octahedral Bond Lengths between the Cations and Their Oxygen Nearest Neighbors for Original $Fd\bar{3}m$, Ordered $P4_122$, and *Imma* Structures of Zn_2SnO_4

	bond lengths (Å)		
bond	$Fd\bar{3}m$ (cubic)	$P4_122$ (tetragonal)	*Imma* (orthorhombic)
Zn^{tetra}—O	2.098	2.004	2.010
Zn^{octa}—O	2.041	2.063	2.120
Sn^{octa}—O	2.041	2.077	2.068

mechanical properties of ZTO nanowires, nanoscale three-point bending tests were performed. To avoid sliding during the bending tests, both ends of the nanowires, which bridged over the trench, were clamped by electron beam induced deposition (EBID) of paraffin (see Supporting Information). Figure 3a shows the AFM image of a well aligned ZTO nanowire over a trench after EBID. Representative force-piezo Z position curves on Si wafer and suspended ZTO nanowires are shown in Figure 3b, which illustrates good linear relationship between the force and piezo Z position up to 1400 nN. On the basis of elastic beam-bending theory, the elastic modulus of ZTO nanowire, E_n can be calculated from[31,32]

$$E_n = k_n L^3/192I \quad (1)$$

where I is the moment of inertia and L is the suspended length of the nanowire. For a round-shaped nanowire, $I = \pi r^4/4$, where r is the radius of the nanowire. k_n, the spring constant of the nanowire, can be obtained from[31,32]

$$k_n = \frac{k_1 k_2}{k_1 - k_2} \quad (2)$$

where k_1 and k_2 are the slopes of the F—Z curves for the Si wafer and the suspended ZTO nanowire shown in Figure 3b, respectively. The average elastic modulus of ZTO nanowires was determined to be 245.5 ± 24.9 GPa, which is a 67.8% increase compared to their bulk counterpart (see Supporting Information). In our DFT calculations, we have determined the elastic constants (C_{11}, C_{22}, and C_{44}) of the ZTO crystal (inverse spinel structure) with the experimentally determined cation ordering and a random cation ordering. The Young's modulus of ZTO crystal was estimated as

$$E = \frac{(C_{11} - C_{12} + 3C_{44})(C_{11} + 2C_{12})}{(2C_{11} + 3C_{12} + C_{44})} \quad (3)$$

It was found that the ZTO crystal with a random cation ordering had a Young's modulus of 164 GPa, whereas the ZTO crystal with cation ordering had a Young's modulus of 243 GPa. Hence, our DFT calculations also suggest that cation ordering could enhance the elastic modulus of ZTO. Specifically, our DFT calculations revealed that cation ordering could cause a significant increase in elastic constant C_{44}, whose value was predicted to change from 76 GPa in the case of random cation ordering to 210 GPa in the case of cation ordering.

The ZTO nanowires exhibited elastic deformation behavior under small applied load. However, increased loading resulted in the crack formation (elastic limit, point 1 in Figure 3d) and propagation and ultimate fracture (flat stage 2 in Figure 3d) of the nanowire. An AFM image of the fractured ZTO nanowire is shown in Figure 3c. To ensure the strength of the tip, a diamond tip with spring constant of 200 N/m was employed to

dx.doi.org/10.1021/nl503077y | *Nano Lett.* 2014, 14, 6505−6509

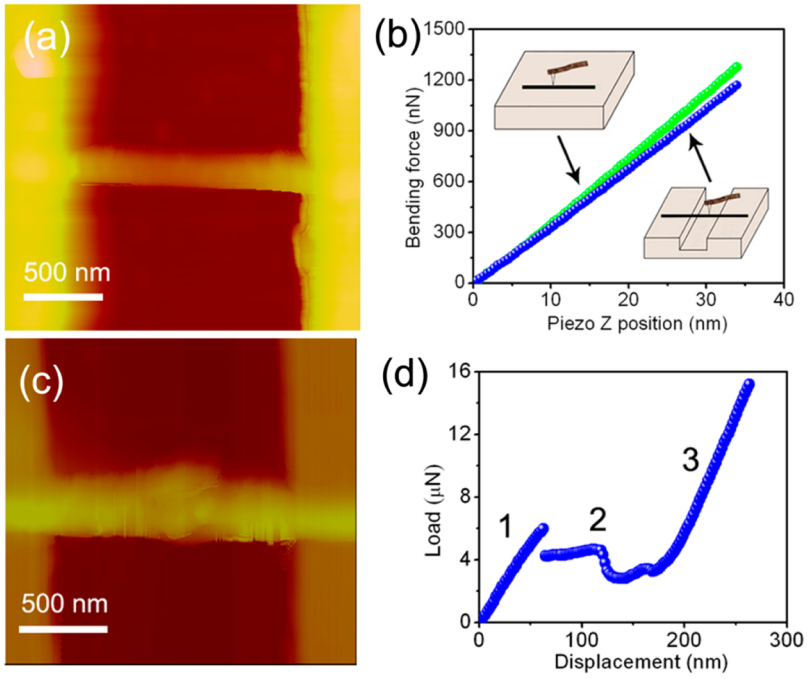

Figure 3. (a) AFM image of an individual ZTO nanowire bridged over the 1.5 μm wide trench after EBID is performed. (b) Representative bending force−piezo position (F−Z) curves for a Si wafer (for calibration) and a suspended nanowire, respectively. (c) AFM image of an individual ZTO nanowire after fracture. (d) Representative full spectrum of force−displacement curve under high loading using a diamond tip.

perform bending tests under high loading. Figure 3d displays a representative force−displacement curve under such high loading bending tests. When the AFM tip continuously pushed the nanowire downward, the nanowire had the maximum strength to keep it from fracture. Once the force applied to the AFM tip reached the nanowire's maximum strength, the nanowire fractured and thus lost its resistance to the AFM tip, leading to a force reduction as the discontinuity between step 1 and step 2. According to the beam-bending theory,[31,32] the fracture strength σ_f can be estimated from the maximum force F_{max} in F−d curves before the onset of crack formation using the following equation:

$$\sigma_f = \frac{F_{max}L}{2\pi r^3} \quad (4)$$

where L is the suspend length and r is the radius of the nanowire. The average fracture strength was measured to be 17.1 ± 5.1 GPa, which does not exceed the theoretical value of $E/10$ for nanowires.[33]

As discussed above, because the electrical conduction mechanism in ZTO is strongly dependent on atom chains along the [110] direction, the formation of Sn atom chains in *Imma* orthorhombic ordered ZTO nanowires (Figure 2e) has important implications on the electrical transport properties of ZTO. To shed light on this, electrical conductivity and electron mobility measurements were performed by fabricating ZTO nanowire FETs, as schematically shown in Figure 4a. Figure 4b shows the current−voltage (I_{ds}−V_{ds}) characteristics of a ZTO nanowire FET at different gate voltages (V_g, from −30 to +30 V with a 10 V step). The inset is the SEM image of the ZTO nanowire FET. Clearly, the conductance of the ZTO nanowire decreases as the gate bias voltage decreases, demonstrating the n-type semiconductor nature of the ZTO nanowires, in accord with bulk ZTO.[26] The extracted conductivity of the ZTO nanowire is 3.6 ± 0.4 S cm^{-1}, which is 10−10^2 times lower than

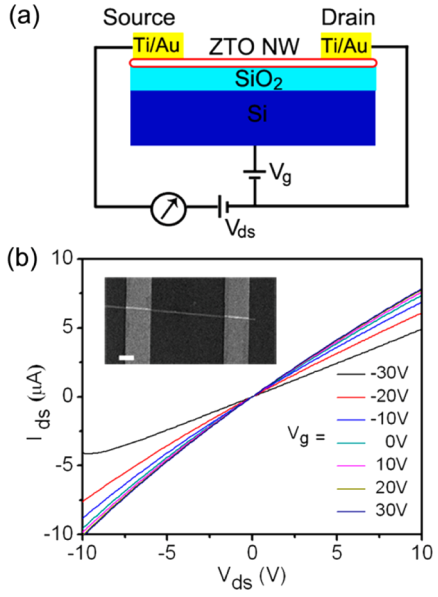

Figure 4. (a) Schematic of ZTO single nanowire field-effect transistor (FET). (b) Gate dependent I−V characteristic of a single ZTO nanowire at room temperature with gate voltages from −30 to +30 V with a 10 V step; inset is the SEM image of the FET. Scale bar, 1 μm.

their bulk counterpart (10^2−10^3 S cm^{-1}). The field-effect mobility of the ZTO nanowires was calculated to be 0.52 ± 0.09 cm^2 V^{-1} s^{-1}, which is much lower than their bulk counterpart (10−10^2 cm^2 V^{-1} s^{-1}).[26]

In summary, we have directly demonstrated the 1:1 ordered occupation of Zn and Sn cations at octahedral B sites with microscopic symmetry transformed from original cubic $Fd\bar{3}m$ to orthorhombic *Imma* group using HAADF-STEM technique coupled with DFT calculations. Such an ordered cation occupation induced a 67.8% increase in the elastic modulus

dx.doi.org/10.1021/nl503077y | *Nano Lett.* 2014, 14, 6505−6509

and 1−2 orders of magnitude lower in the electric conductivity and electron mobility compared to their bulk counterpart.

■ ASSOCIATED CONTENT

Supporting Information

Experimental details for the device preparation, characterization, and additional supporting data. This material is available free of charge via the Internet at http://pubs.acs.org.

■ AUTHOR INFORMATION

Corresponding Author

*E-mail: lixiao@cec.sc.edu.

Present Addresses

[§]Institute of Physics, Chinese Academy of Sciences, Beijing 100190, China.

[∥]School of Optical and Electronic Information, Innovation Institute, Huazhong University of Science and Technology, 1037 Luoyu Rd, Wuhan 430074, China.

Notes

The authors declare no competing financial interest.

■ ACKNOWLEDGMENTS

We would like to thank Dr. Douglas Blom in the Electron Microscopy Center of the University of South Carolina for his extensive help on STEM characterization. This work was supported by the National Science Foundation (CMMI-1129979) and the Army Research Office under Agreement/Grant W911NF-08-0299.

■ REFERENCES

(1) Baltzer, P. K.; Lehmann, H. W.; Robbins, M. *Phys. Rev. Lett.* **1965**, *15* (11), 493−495.

(2) Sickafus, K. E.; Wills, J. M.; Grimes, N. W. *J. Am. Ceram. Soc.* **1999**, *82* (12), 3279−3292.

(3) Segev, D.; Wei, S. H. *Phys. Rev. B* **2005**, *71* (12), 125129.

(4) Kawazoe, H.; Ueda, K. *J. Am. Ceram. Soc.* **1999**, *82* (12), 3330−3336.

(5) Margulies, D. T.; Parker, F. T.; Rudee, M. L.; Spada, F. E.; Chapman, J. N.; Aitchison, P. R.; Berkowitz, A. E. *Phys. Rev. Lett.* **1997**, *79* (25), 5162−5165.

(6) Reffas, M.; Bouhemadou, A.; Khenata, R.; Ouahrani, T.; Bin-Omran, S. *Phys. B* **2010**, *405* (18), 4079−4085.

(7) Garlea, V. O.; Jin, R.; Mandrus, D.; Roessli, B.; Huang, Q.; Miller, M.; Schultz, A. J.; Nagler, S. E. *Phys. Rev. Lett.* **2008**, *100* (6), 066404.

(8) Rasmussen, M. K.; Foster, A. S.; Hinnemann, B.; Canova, F. F.; Helveg, S.; Meinander, K.; Martin, N. M.; Knudsen, J.; Vlad, A.; Lundgren, E.; Stierle, A.; Besenbacher, F.; Lauritsen, J. V. *Phys. Rev. Lett.* **2011**, *107* (3), 036102.

(9) Murphy, S. T.; Uberuaga, B. P.; Ball, J. B.; Cleave, A. R.; Sickafus, K. E.; Smith, R.; Grimes, R. W. *Solid State Ionics* **2009**, *180* (1), 1−8.

(10) Altman, E. I.; Schwarz, U. D. *Adv. Mater.* **2010**, *22* (26−27), 2854−2869.

(11) Stewart, S. J.; Figueroa, S. J. A.; Ramallo López, J. M.; Marchetti, S. G.; Bengoa, J. F.; Prado, R. J.; Requejo, F. G. *Phys. Rev. B* **2007**, *75* (7), 073408.

(12) Chappert, J.; Frankel, R. B. *Phys. Rev. Lett.* **1967**, *19* (10), 570−572.

(13) Grimes, R. W.; Anderson, A. B.; Heuer, A. H. *J. Am. Chem. Soc.* **1989**, *111* (1), 1−7.

(14) Ivanov, V. G.; Abrashev, M. V.; Iliev, M. N.; Gospodinov, M. M.; Meen, J.; Aroyo, M. I. *Phys. Rev. B* **2010**, *82* (2), 024104.

(15) Seko, A.; Oba, F.; Tanaka, I. *Phys. Rev. B* **2010**, *81* (5), 054114.

(16) Stevanovic, V.; d'Avezac, M.; Zunger, A. *J. Am. Chem. Soc.* **2011**, *133* (30), 11649−11654.

(17) Haas, C. *J. Phys. Chem. Solids* **1965**, *26* (8), 1225−1232.

(18) Landau, L. D.; Lifshitz, E. M. *Statistical Physics*; Pergamon Press: Oxford, U.K., 1959.

(19) Chen, J. H.; Weidner, D. J.; Parise, J. B.; Vaughan, M. T.; Raterron, P. *Phys. Rev. Lett.* **2001**, *86* (18), 4072−4075.

(20) Millard, R. L.; Peterson, R. C.; Hunter, B. K. *Am. Mineral.* **1995**, *80* (9−10), 885−896.

(21) Wechsler, B. A.; Vondreele, R. B. *Acta Crystallogr., Sect. B: Struct. Sci.* **1989**, *45*, 542−549.

(22) Nellist, P. D.; Chisholm, M. F.; Dellby, N.; Krivanek, O. L.; Murfitt, M. F.; Szilagyi, Z. S.; Lupini, A. R.; Borisevich, A.; Sides, W. H.; Pennycook, S. J. *Science* **2004**, *305* (5691), 1741−1741.

(23) Krivanek, O. L.; Chisholm, M. F.; Nicolosi, V.; Pennycook, T. J.; Corbin, G. J.; Dellby, N.; Murfitt, M. F.; Own, C. S.; Szilagyi, Z. S.; Oxley, M. P.; Pantelides, S. T.; Pennycook, S. J. *Nature* **2010**, *464* (7288), 571−574.

(24) Chung, S.-Y.; Choi, S.-Y.; Yamamoto, T.; Ikuhara, Y. *Phys. Rev. Lett.* **2008**, *100* (12), 125502.

(25) Minami, T. *MRS Bull.* **2000**, *25*, 38−44.

(26) Nomura, K.; Ohta, H.; Ueda, K.; Kamiya, T.; Hirano, M.; Hosono, H. *Science* **2003**, *300* (5623), 1269−1272.

(27) Tan, B.; Toman, E.; Li, Y. G.; Wu, Y. Y. *J. Am. Chem. Soc.* **2007**, *129* (14), 4162−4163.

(28) Rong, A.; Gao, X. P.; Li, G. R.; Yan, T. Y.; Zhu, H. Y.; Qu, J. Q.; Song, D. Y. *J. Phys. Chem. B* **2006**, *110* (30), 14754−14760.

(29) Seko, A.; Yuge, K.; Oba, F.; Kuwabara, A.; Tanaka, I. *Phys. Rev. B* **2006**, *73* (18), 184117.

(30) Bao, L. H.; Zang, J. F.; Li, X. D. *Nano Lett.* **2011**, *11* (3), 1215−1220.

(31) Bhushan, B.; Li, X. D. *Int. Mater. Rev.* **2003**, *48* (3), 125−164.

(32) Wu, B.; Heidelberg, A.; Boland, J. J. *Nat. Mater.* **2005**, *4* (7), 525−529.

(33) Barrett, C. R.; Nix, W. D.; Tetelman, A. S. *The Principles of Engineering Materials*; Prentice- Hall: Englewood Cliffs, NJ, 1973.